Rheological and small-angle neutron scattering studies of aqueous solutions of branched PEO-PPO-PEO copolymers

Christelle Perreur, Jean-Pierre Habas, Jean Peyrelasse,* and Jeanne François
Laboratoire de Physicochimie des Polymères, UMR 5067, Université de Pau et des Pays de l'Adour, Avenue de l'Université, 64000 Pau, France

Alain Lapp
Laboratoire Léon Brillouin, CEA Saclay, 91191 Gif-sur-Yvette, Cedex, France
(Received 4 August 2000; published 27 February 2001)

Tetronic® 908 is a four-branched copolymer comprised of polyethylene oxide (PEO) and polypropylene oxide (PPO) blocks fixed on an aliphatic diamine. In aqueous solution, this polymer has an amphiphilic character due to the difference in PEO and PPO solubilities with increase in temperature. This system presents interesting rheological properties depending on the polymer concentration in solution and temperature. At low temperatures and/or concentrations, the solution behaves as a Newtonian fluid. For a weight percentage p comprised between 2% and 22%, the viscosity of the solution goes through a maximum. Small-angle neutron scattering experiments show that the increase in viscosity is due to progressive aggregation of chains. For weight percentages higher than $p=22\%$, the viscosity of the system diverges and the mixture becomes gel-like. In fact, spectromechanical measurements show that the solution behaves as an entangled polymer with a high relaxation time in the flow zone. Small-angle neutron scattering (SANS) studies of the same solution reveal the presence of several peaks indicating that the micelles are organized in a cubic structure. We have developed a model that suitably describes the SANS curves of this system in the region where micelles are formed. Our model considers that micelles are trilayered spherical entities that coexist with unimers by obeying an equilibrium reaction. Moreover, it allows the calculation of several parameters such as the volume fraction of micelles, their size, and composition. The evolution of these parameters with temperature and polymer concentration is detailed. Comparisons with literature models are presented and discussed. This compilation of results has permitted the establishment of precise relations between the structure of this polymer in solution and its rheological properties.

DOI: 10.1103/PhysRevE.63.031505 PACS number(s): 61.25.Hq, 61.12.Ex, 83.85.Jn, 83.85.Cg

I. INTRODUCTION

Many reports have been published over the last decade on the aqueous solution properties of polyethylene oxide (PEO) and polypropylene oxide (PPO) block copolymers. The most commonly studied polymers have the structure of type PEO-PPO-PEO. These compounds are nonionic surfactants and have a wide variety of application in fields ranging from medicine to petroleum industry. At low temperatures, both PEO and PPO blocks are water soluble; however, when the temperature is increased, PPO becomes insoluble. This amphiphilic character gives rise to a wide range of structures, depending on various parameters such as the length of the PEO and PPO sequences, temperature, and polymer concentration. At low temperatures and concentrations, the copolymer exists in solution as individual molecules, i.e., unimers. When the temperature is increased, these unimers self-associate to form micelles. If the concentration is high enough, a transition is observed to a state of high viscosity commonly called ''gel'' and may be due to the organization of micelles into pseudocrystalline phases (fcc, bcc, hexagonal, lamellar or rods).

Most of the literature deals with linear polymers such as Pluronic® (BASF) or Poloxamers® (ICI). Many experimental techniques have been used such as measurement of surface tension [1–3], differential scanning calorimetry [4–6], light scattering [7–10], viscosimetry [11–13], and ultrasonic velocity measurements [14]. Small angle neutron scattering (SANS) [15–20] and small-angle x-ray scattering [6,10,21–23] seem to be the most appropriate techniques for obtaining precise information on the structure of such solutions and organized phases. An analysis of the literature data exposes the complex behavior of these systems. This complexity is often apparent in the contradictory conclusions proposed by authors. In particular, the existence of an enthalpic effect close to the temperature of micellization is not clear. Hvidt shows the occurrence of an endothermic peak in a calorimetric study of a Pluronic $(EO)_{28}(PO)_{48}(EO)_{28}$ [4]. The works of Glatter *et al.* on a Pluronic $(EO)_{27}(PO)_{39}(EO)_{27}$, confirmed this result [6]. Wanka, Hoffmann, and Ulbricht also observe this phenomenon with Pluronic F127, $(EO)_{100}(PO)_{65}(EO)_{100}$ but attributed it to the dehydration of PO units, whereas the order-disorder transition was judged to be athermic [1]. Curiously, Lenaerts *et al.* do not record any thermal particularity with the same polymer [5]. Similar discrepancies are observed also when considering the structure of organized phases. SANS studies performed by Prud'homme, Wu, and Schneider on Pluronic F127 solutions seem to indicate the formation of a simple cubic or bcc network [24]. This conclusion is in agreement with Mortensen's work [17] but Wu,

*Author to whom correspondence should be addressed. Email address: jean.peyrelasse@univ-pau.fr

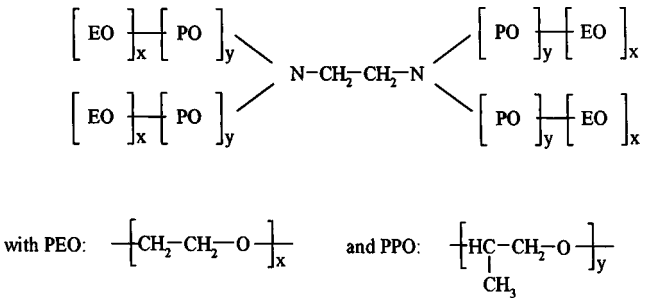

FIG. 1. Chemical structure of Tetronic 908.

Liu, and Chu [22] suggest, for the same polymer, that the structure is fcc type. Alternatively, King *et al.* point out a transition from spherical to cylindrical micelles [12].

The BASF company has also commercialized a four-branched copolymer named Tetronic, comprised of PEO and PPO blocks fixed on an aliphatic diamine. These types of surfactants have been poorly studied until now. Our work aims to correlate viscosimetric and rheological results with structural information derived from small-angle neutron scattering experiments. In particular, our study deals with the transition zone above the critical micellization temperature (CMT) where equilibrium between unimers and micelles should exist. Indeed, if many authors have determined the temperature domain associated with unimers $\rightleftharpoons$ micelles transitions, the equilibrium state has never been fully characterized [6,8,25–27].

II. EXPERIMENTAL SECTION

A. Samples

Tetronic from BASF is composed of polyoxyethylene (PEO) and polyoxypropylene (PPO) blocks with an aliphatic diamine. In this paper, we have studied the properties of T908 ($M_w = 25000\ \mathrm{g\,mol^{-1}}$) for which the number of EO and PO units per branch are, respectively, $x = 114$ and $y = 21$ (Fig. 1). This polymer was used without further purification. Aqueous solutions were prepared at low temperatures under stirring, using twice-distilled water for all rheological experiments and deuterated water D_2O for small-angle neutron scattering studies. For this study, the weight percentage p of polymer is comprised between 1% (w/w) and 50% (w/w) and the temperature range from 5 °C to 80 °C.

B. Experimental methods

1. Rheology

Capillary rheometer: Viscosimetric measurements were performed using Ubbelohde capillary tubes: the measurement of flow time between two reference marks made it possible to determine the kinematic viscosity η_k of solutions. In order to calculate the dynamic η and reduced η_r viscosities of solutions, we have measured their density d using an automatic densimeter ANTON PAAR DMA 45®. It can be noted that knowledge of density also permits the determination of the concentration of polymer in solution ($\mathcal{C}$ in $\mathrm{g\,cm^{-3}}$).

Dynamic stress rheometer. The dynamic rheological properties were studied using a rheometric scientific DSR®. This apparatus is a stress-controlled rheometer with Couette geometry. All experiments were performed within the angular-frequency range from $10^{-4}\ \mathrm{rad\,s^{-1}}$ to $10^{2}\ \mathrm{rad\,s^{-1}}$ and the stress was set to work in the linear region (i.e., moduli independent of stress)

2. Small angle neutron scattering

SANS experiments were performed at the Laboratoire Léon Brillouin, CE de Saclay (France) on the PAXY spectrometer. A wavelength of 8 Å (with a resolution of 10%) was selected, and an effective distance between the sample and the detector was 3.1 m. This allowed for a momentum transfer range of 0.06–0.9 $\mathrm{nm^{-1}}$. Quartz cells were used with 2-mm or 1-mm path lengths. Data correction allowed for sample transmission and detector efficiency. The efficiency of the detector was taken into account with H_2O scattering. Absolute intensities were obtained by reference to the attenuated direct beam, and the scattering of pure solvent was subtracted. Finally, intensities were corrected for a small solute incoherent contribution. The scattering patterns of our samples were all isotropic and the one-dimensional data sets were generated by circular integration of the corresponding two-dimensional patterns.

3. Static light scattering

Static light diffusion experiments were performed on a SEM 633 apparatus. The light source used was a vertically polarized He-Ne laser (632.8 nm). The polymer solution was prepared using fresh thrice-distilled water. All measurements were made at a fixed direction (90°) on a wide range of temperatures from 15 °C to 80 °C.

III. RESULTS AND DISCUSSION

A. Rheological studies

1. Viscosimetry

Viscosimetric studies of aqueous solutions of T908 show that the general behavior of the system was strongly dependent on the weight-percentage value (p) of polymer in solution. For p ranging between 10% and 22%, the viscosity η_k of the solution first decreased as temperature increased as observed for classical liquids. Then, it passed through a maximum (Fig. 2). At higher temperatures, the usual behavior prevailed and the viscosity decreased again. Figure 3 shows the variations of $\ln(\eta_k)$ according to the reciprocal of absolute temperature for $p = 20\%$. In the low-temperature range, up to the temperature T_1 the plot is linear, the solution behaved as a classical liquid.

For $p = 5\%$, the kinematic-viscosity curve presented only a single inflection point. Plotting, however, the variations in reduced viscosity η_r, with temperature, there is a noticeable maximum in the same thermal region (Fig. 4). For weight percentages lower than $p = 2\%$, no anomalies were detected.

For p higher than 22%, we did not observe any maxima on the viscosity curves. But, above a well-defined tempera-

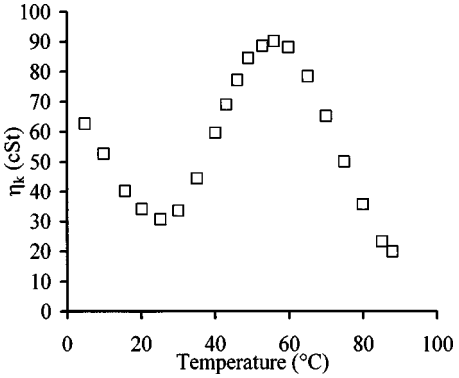

FIG. 2. Evolution of kinematic viscosity of a 20% solution with temperature.

ture labeled T_c, depending on concentration, the viscosity of the solution increased abruptly. An example is shown in Fig. 5 for $p=30\%$. Above T_c, the mixture is unable to flow and, at first sight, it becomes gel-like.

Taking into account the published literature for similar polymeric solutions [17], initial explanations can be proposed to understand the results of the viscosimetric characterization. We can assume that, at low temperatures, the sample is a solution of unimers. At temperatures higher than the critical value T_1, the hydrophobicity of PPO is sufficient such that micelles form. The increase of the volume fraction of micelles subsequently induces a rise in viscosity (for $p>2\%$). T_1 can be considered as the CMT for a given concentration of polymer in solution.

The interpretation of the viscosity maximum is more difficult. Two hypotheses are suggested.

(i) The volume fraction of micelles does not change and the viscosity decreases with increasing temperature as observed for most liquids.

(ii) The volume fraction of micelles goes through a maximum.

SANS studies of the solutions should provide detailed information allowing us to determine which hypothesis is correct.

When $p>22\%$, the volume fraction of the micelles was great enough to produce a gel or an organized phase.

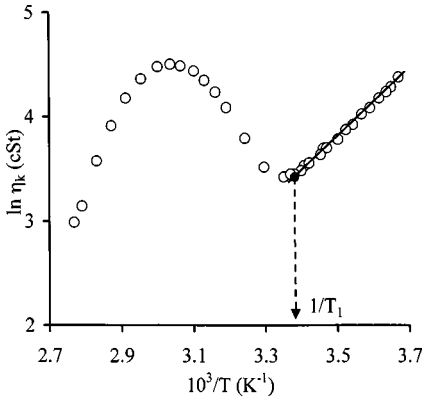

FIG. 3. Variations of log of kinematic viscosity of a 20% solution as a function of the reciprocal of absolute temperature.

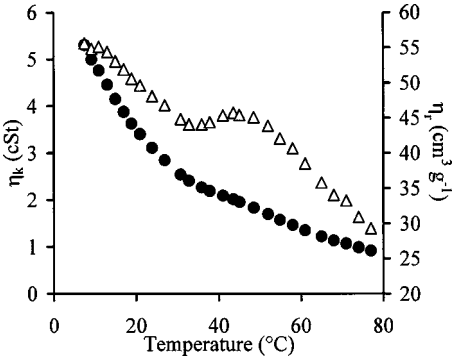

FIG. 4. Evolution of kinematic (●) and reduced viscosities (△) of a 5% solution with temperature.

Determination of critical temperatures T_1 and T_c allows a phase diagram to be drawn that according to the hypothesis noted above, can be divided into three zones (Fig. 6). In the first one, the solution contains only unimers; in the second, there is coexistence of unimers and micelles; and the third is representative of a gel-like system.

To assess these results, light-scattering experiments for two solutions (5% and 10%) were performed. Figure 7 presents the variations in the scattered intensities with temperature for a 10% solution. It can be noted that at low temperatures, the intensity remained quasiconstant. At $T>30\,°C$, the intensity strongly increased. This phenomenon was due to micellization. The value of the CMT measured by this method is in good agreement with the one determined by the viscosimetric study as shown in Fig. 6.

We also performed calorimetric analysis on T908 aqueous solutions to explore possible enthalpic phenomena associated with the transition at the CMT or at T_c. Our experiments did not show any processes even for concentrated solutions.

2. Rheology

Spectromechanical analyses of a 30% solution of Tetronic 908 permitted a study of the evolution of the rheological properties of the system with temperature. Below 35 °C, the viscosity of the solution was very low and outside of the range of sensitivity of the apparatus. However, between

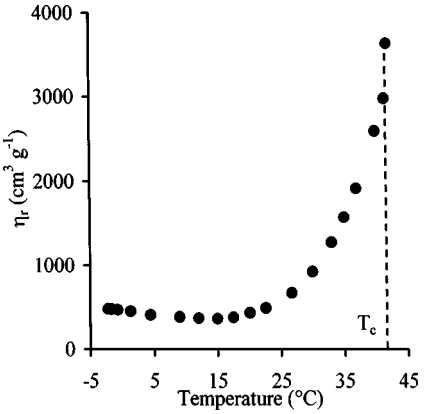

FIG. 5. Temperature dependence of reduced viscosity of a 30% solution.

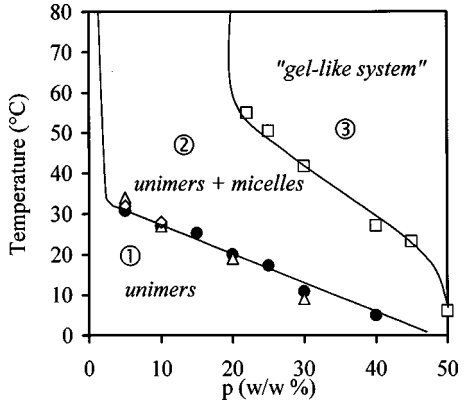

FIG. 6. Phase diagram of aqueous solutions of Tetronic 908: ●, miscellisation temperature determined by viscosimetry; ◇, miscellization temperature determined by static light scattering; △, miscellization temperature determined by SANS; □, transition temperature to ''gel-like system.''

35 °C, and 40 °C, and in the frequency range used, the flow zone of the polymeric solution is described: G' was proportional to ω^2 and G'' to ω over a wide frequency domain. For temperatures above 41 °C, the solution behaved as an entangled polymer. This was indicated by the presence of a crossover on the rheological curves (Fig. 8). As the temperature increased, the crossover was shifted to lower frequencies. It is important to note that the flow zone is always detected. So, the structure of the solution in zone 3 of the phase diagram is not that of a gel, and this is contrary to assessments of various authors [3,7,11,24].

Between 35 °C and 40 °C, the analysis of the here described experiments leads to the determination of viscosity $\eta_0 = \lim_{\omega \to 0} G''/\omega$. The values of viscosity have been corrected with the variations in density of the solution with temperature. Then, they have been compared to those determined by the capillary method. The agreement between the results from the two techniques is very good and assesses that in this thermal range, the solutions behaved as Newtonian liquids (Fig. 9).

Plotted also on Fig. 9, for $T > 41$ °C are the variations of rubbery plateau values G_e (arbitrarily defined as the value of G' at 100 rad s^{-1}) according to temperature. A strong increase occurs around $T_c = 41$ °C, but beyond, G_e is practically constant. The intersection of the two linear parts of the curve $G_e = f(T)$ defines a temperature that corresponds to that obtained for the divergence of viscosity. It should be noted that the transition was extremely rapid. For example, the relaxation time in the terminal zone, taken equal to the inverse of the angular frequency at the crossover is close to 1 s at $T = 41.2$ °C whereas it exceeds 600 s at $T = 42$ °C (Fig. 8).

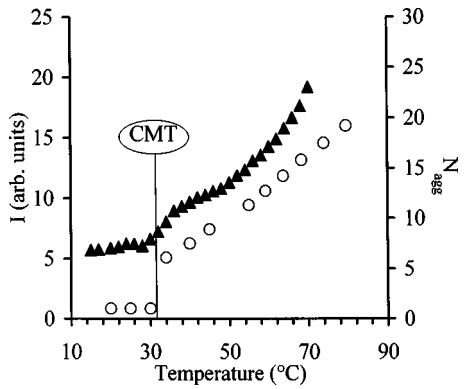

FIG. 7. Intensity of light scattering (▲) and evolution of aggregation number (○) of a 10% solution with temperature.

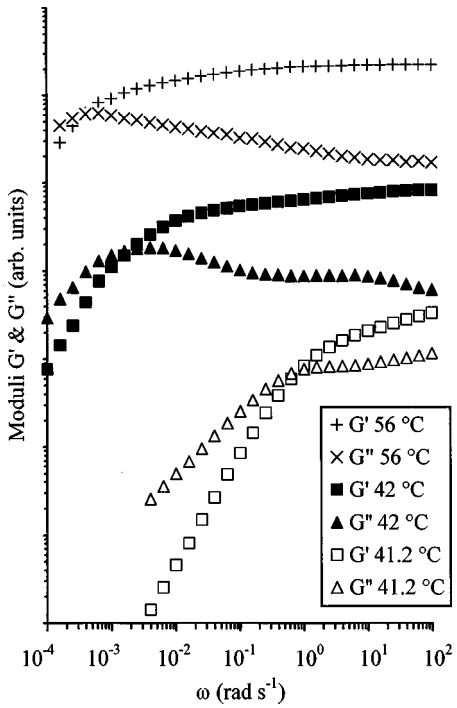

FIG. 8. Spectromechanical analysis of a 30% solution: the effect of temperature.

B. SANS studies

1. Experimental results

In order to detail more precisely the solutions structures, small-angle neutron scattering measurements at different temperatures and concentrations were performed in all parts of the phase diagram.

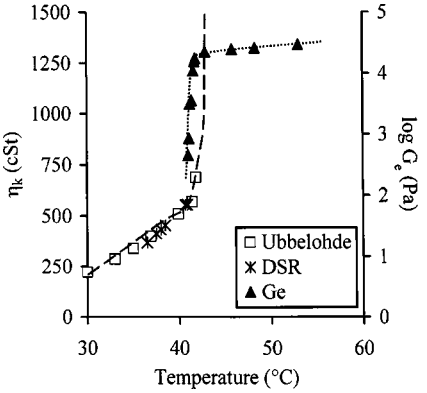

FIG. 9. Evolutions of the viscosity and equilibrium modulus of a 30% solution.

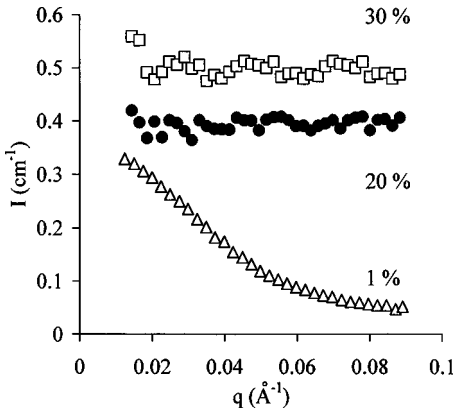

FIG. 10. Variations in scattered intensity of different solutions: △, $p=1$; ●, $p=20\%$; □, $p=30\%$.

For dilute solutions ($p=1\%$) and in zone 1 of the phase diagram of Fig. 6, the curve of scattered intensity $I(q)$ seemed to vary as a Debye function. However, the concentration was still too high to allow the calculation of the radius of gyration and molar weight of unimers. In the same zone of the phase diagram, but for concentrated solutions, it was noticeable that the scattered intensity remains weak but above all, was independent of q. This result was very important because it proved that concentrated solutions of unmicellized polymer behave as homogenous mixtures. Figure 10 allowed a comparison between concentrated solutions ($p=20\%$, $p=30\%$) with a dilute system ($p=1\%$).

For systems in zone 2 or 3 of the phase diagram, the curve $I(q)$ presented a maximum whose intensity grew with temperature. It is worth considering this in light of Figs. 11 and 12 that show the variations in the scattered intensity according to the amplitude q of the scattering vector, for two solutions ($p=20\%$ and $p=30\%$, respectively) and at different temperatures. Similarly, Fig. 13 represents the variations of

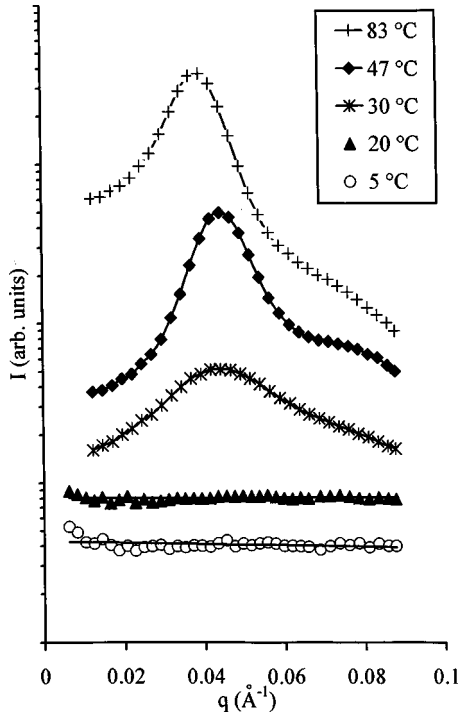

FIG. 11. Effect of temperature on scattered intensity of a 20% solution (the curves have been arbitrarily shifted along the y axis).

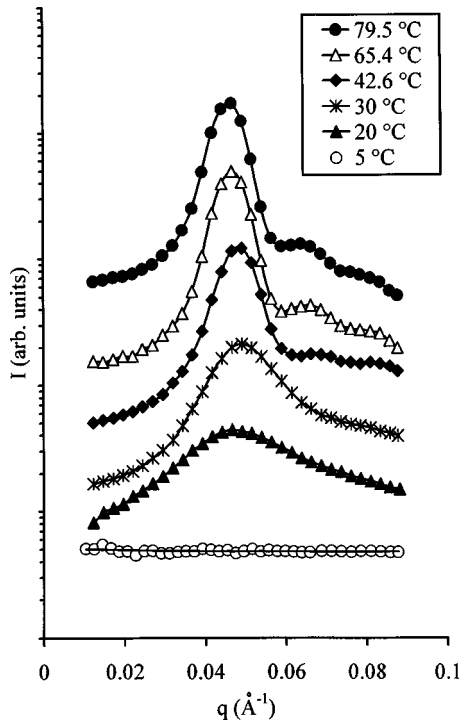

FIG. 12. Effect of temperature on scattered intensity of a 30% solution (the curves have been arbitrarily shifted along the y axis).

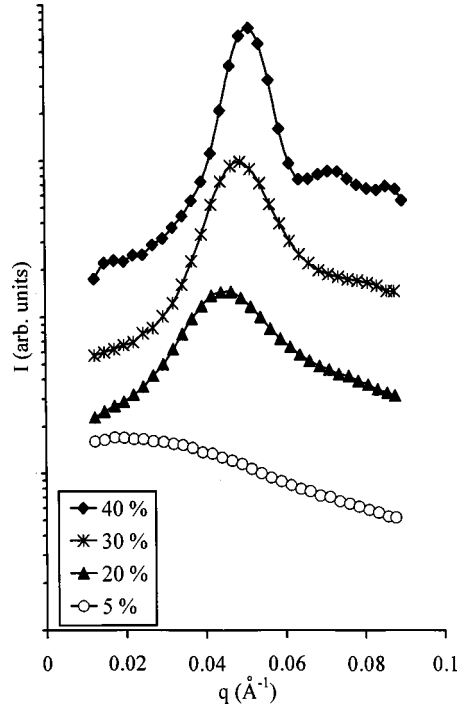

FIG. 13. Evolution of scattered intensity with concentration of T908 in solution at $T=35\,°C$ (the curves have been arbitrarily shifted along the y axis).

the scattered intensity for different percentages of polymer at a constant temperature (35 °C). In zone 3 of the phase diagram, some small peaks of higher order appeared on the curve of scattered intensity. This phenomenon clearly appeared for $p=30\%$ at $T \geqslant 42.6\,^{\circ}\mathrm{C}$ (Fig. 12) and for $p=40\%$ at 35 °C (Fig. 13) and follows the transition to an organized phase. The organization of the micelles induced a high viscosity system.

2. Literature models

A great deal of work has been devoted to the interpretation of results from neutron scattering experiments with linear PEO-PPO-PEO systems. When concentration of polymer in solution is low, the scattered intensity is mainly governed by the form factor $P(q)$. When concentration increases, intermicellar correlations become significant and for a monodisperse system of particles, $I(q)$ can be written as the product of the particle form factor and the structure factor $S(q)$

$$I(q)=N\Delta\rho^2 P(q)S(q),$$

where N is the number density of scatterers and $\Delta\rho^2$ the contrast factor.

The interparticle interference $S(q)$ may be calculated by assuming an interaction potential. For the hard sphere model, the structure factor is well known

$$S(q)=\frac{1}{1+24\phi_{\mathrm{hs}}G(x,\phi_{\mathrm{hs}})/x},$$

where $x=2qR_{\mathrm{hs}}$, R_{hs} is the hard sphere interaction radius, ϕ_{hs} is the hard sphere volume fraction, and $G(x,\phi_{\mathrm{hs}})=A(x)+B(x)+C(x)$, where

$$A(x)=\frac{\alpha}{x^2}[\sin x - x\cos x],$$

$$B(x)=\frac{\beta}{x^3}[2x\sin x+(2-x^2)\cos x-2],$$

$$C(x)=\frac{\gamma}{x^5}[-x^4\cos x+4(3x^2-6)\cos x + 4(x^3-6x)\sin x+24],$$

with

$$\alpha=\frac{(1+2\phi_{\mathrm{hs}})^2}{(1-\phi_{\mathrm{hs}})^4},\quad \beta=\frac{-6\phi_{\mathrm{hs}}(1+\phi_{\mathrm{hs}}/2)^2}{(1-\phi_{\mathrm{hs}})^4},$$

$$\gamma=\frac{\phi_{\mathrm{hs}}}{2}\frac{(1+2\phi_{\mathrm{hs}})^2}{(1-\phi_{\mathrm{hs}})^4}.$$

Liu, Chem, and Huang used a more complex model of adhesive hard spheres that took into account the possible attractive interactions occurring between micelles. This model required the introduction of two additional parameters, the surface adhesion potential and the fractional surface layer thickness [18].

The form factor depends on the model selected to describe the micelles. Fundamental discrepancies are found between different authors. The simplest model is that of Mortensen and co-workers who assume a monodisperse suspension of dense spheres with a sharp interface [15,16]. Mortensen and co-workers have postulated that the core of radius R_c holds the totality of PPO units and a small percentage of PEO, which is not possible to detect since the scattering length density of EO and PO are close. The major part of PEO forms a hydrated corona, but the authors neglected its presence in their calculations. Then, the form factor $P(q)$ is that of a hard sphere and is given by the equation

$$P(q)=\left[\frac{4\pi}{3}R_c^3\frac{3j_1(qR_c)}{qR_c}\right]^2.$$

j_1 is the first order spherical Bessel function defined by $j_1(x)=(\sin x - x\cos x)/x^2$.

In their model, the various adjustable parameters are the equivalent hard sphere radius R_{hs}, the volume fraction of hard sphere ϕ_{hs}, and the core radius R_c. The analysis presents the advantage of not requiring knowledge of the number of unimers in micelles. But, it does not allow calculations of the aggregation number. The main defect was the omission of the corona whose contrast can hardly be considered equal to that of water, even when the latter contains the majority of PEO units.

Goldminst *et al.* used a two-shell model where the micelle was assimilated to a core of radius R_c surrounded by a corona of radius R_m [19,20]. The authors set different hypotheses: (i) the radius R_m of the micelle was assumed identical to the radius of the hard sphere $R_m=R_{\mathrm{hs}}$; (ii) the scattering length densities (SLDs) of PO and EO are equal; and (iii) water is present both in the core and the corona of the micelle.

Liu *et al.* used also a two-shell model in which the core of the micelle was made of PO units under close-packing conditions and the corona was considered of an homogenous mixture of PEO and water. They assume that the entire polymer was micellized.

The previous models present some problems. The models of Goldminst *et al.* and Liu's require the knowledge of the aggregation number, which can only be determined if we know the equilibrium of unimers and micelles at each temperature and concentration. Goldminst supposes that at a fixed temperature, the fraction of unimers is independent of the initial concentration of the solution and is equal to CMC. If this hypothesis may be correct for poorly concentrated solutions, we will see later that it may not be relevant to the polymer that we have studied.

We have tried to fit the neutron scattering curves with the different models previously outlined. Figure 14 shows that the models of Mortensen and co-workers and Goldminst *et al.* models correctly describe the position and the amplitude of the peak. As these parameters are governed by the structure factor, we can assume that these models give good estimates of the volume fraction and radius of the micelles. Both models considerably deviate, however, from experimental data at low and high values of q. This shows that the

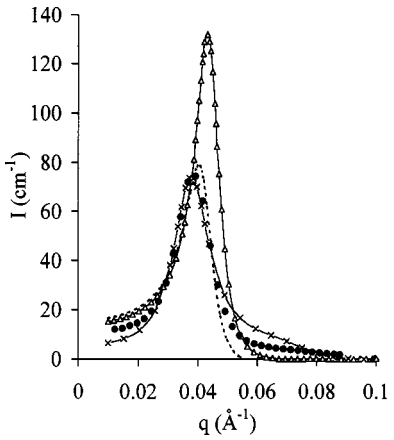

FIG. 14. Comparison of different literature models: application to a 20% solution at $T=83°C$. ●, experimental points; -△-, Liu's model; — — —, model of Goldminst *et al.*; -×- model of Mortensen *et al.*

micellar structure is not well described. As regards Liu's model, the peak is overestimated, which is probably due to not taking into account the important fraction of unmicellized polymer.

3. Our model

In order to explain better our experimental results, here we propose a quite different model. It is based on three-shell model with four adjustable parameters. For this multilayer model we can write [28]

$$P(q)\Delta\rho^2=\sum_1^3\left(\frac{4\pi}{3}R_i^3(\rho_i-\rho_{i+1})\frac{3j_1(qR_i)}{qR_i}\right)^2,$$

where j_1 is the first order spherical Bessel function previously defined, R_i is the radius of the ith layer and ρ_i its SLD. For $i=3$, ρ_4 is the SLD of the solvent:

The hypotheses of our model are as follow: (i) all micelles are identical; (ii) the core of radius R_1 contains the totality of micellized PPO in close-packing conditions; (iii) the first layer of thickness R_2-R_1 is constituted by a fraction χ of PEO units in the micelles; and (iv) the corona of external radius $R_m=R_{\rm hs}$ is an homogenous mixture of water and residual PEO units.

To calculate the structure factor $S(q)$, we have used the equations previously described.

The four parameters are the volume fraction ϕ, the radius R_m of micelles, the fraction χ of PEO in the dense layer, and the concentration C_m of micellized polymer ($\mathrm{g\,cm^{-3}}$). C is the total concentration of polymer in the solution ($\mathrm{g\,cm^{-3}}$).

In a unit volume of sample, the number of micelles is

$$N_m=\frac{3\phi}{4\pi R_m^3}.$$

Then, it is possible to determine (i) the aggregation number,

$$N_{\rm agg}=\frac{C_mN_a}{N_mM_w}$$

where M_w is the molar weight of the polymer and N_a the Avogadro number; (ii) the radius of the core R_1,

$$R_1=\left(\frac{3N_{\rm agg}V_{\rm ppo}}{4\pi}\right)^{1/3},$$

where $V_{\rm ppo}$ is the volume of PO in a Tetronic molecule; and (iii) the external radius R_2 of the dense layer of PEO,

$$R_2=\left(\frac{3>xN_{\rm agg}V_{\rm peo}}{4\pi}+R_1^3\right)^{1/3},$$

where $V_{\rm peo}$ is the volume of EO in a Tetronic molecule.

In the corona, the volume fraction $\phi_{\rm eo}$ of PEO is defined by

$$\phi_{\rm eo}=\frac{3N_{\rm agg}V_{\rm peo}(1-\chi)}{4\pi(R_m^3-R_2^3)}.$$

The various SLDs can easily be calculated (i) for the core, $\rho_{\rm po}=b_{\rm po}/v_{\rm po}$, where $b_{\rm po}$ is the scattering length of PO and $v_{\rm po}$ its molecular volume, (ii) for the dense layer of PEO, $\rho_{\rm eo}=b_{\rm eo}/v_{\rm eo}$, where $b_{\rm eo}$ is the scattering length of EO and $v_{\rm eo}$ its molecular volume; and (iii) for the corona, $\rho_c=\phi_{\rm eo}\rho_{\rm eo}+(1-\phi_{\rm eo})\rho_w$ where ρ_w is the scattering length density of D_2O.

We have previously showed that a concentrated solution of unimers behaves as a homogeneous medium and that the scattered intensity remains weak and can be neglected. However, all unimers are not in micelles. So, it is necessary to take into account their concentration in the continuous phase in order to calculate the scattering length density of the solvent.

The number of molecules of polymer (unimers) N_p and the volume of water V_w in the continuous phase are $N_p=(C-C_m)N_a/M_w$ and $V_w=1-C/d_p-V_{\rm em}$, respectively, with d_p the density of pure polymer, $V_{\rm em}$ the total volume of water contained in micelles. It is possible to determine the volume fractions $f_{\rm po}$, $f_{\rm eo}$, and f_w of PPO, PEO, and D_2O, respectively, in the continuous phase. Then, the scattering length density of the solvent can be calculated as $\rho_s=f_{\rm po}\rho_{\rm po}+f_{\rm eo}\rho_{\rm eo}+f_w\rho_w$ with $f_{\rm po}+f_{\rm eo}+f_w=1$. It should be noted that $f_{\rm po}$ and $f_{\rm eo}$ are not independent.

We have used the same values of scattering length densities of EO, PO, and D_2O as Liu (Table I).

By numerical fitting, we have determined the best values of the four parameters for all studied solutions. It is worth noting that for all concentrations and at each temperature, the agreement between the model and the experimental data is very good. Two examples are proposed in Fig. 15. The convergence in the iteration process is very fast even if the initial values of the adjustable parameters are far from the final result.

TABLE I. Molecular volumes and scattering lengths of EO, PO, and solvent.

Unit	Molecular weight ($g\,mol^{-1}$)	Molecular volume ($Å^3$)	SLD (10^{-5} Å)
EO	44	72.4	4.14
PO	58	95.4	3.31
Solvent	20	30.3	19.15

In zone 3 of the phase diagram, peaks of higher order appear, which are induced by the occurrence of local organization. However, the intensity of these peaks remains very low. So, it can be reasonably thought that the height of the main peak is weakly influenced by this phenomenon. Therefore, we have also analyzed the results of zone 3 of the phase diagram by cutting the experimental curves after the first peak. Our model satisfactorily describes the position and amplitude of the first peak and well fits the experimental values at low q.

In addition to the internal structure of the micelles, our model gives fundamental information such as the aggregation number, the concentration of micellized polymer, and the volume fraction of micelles as a function of temperature and initial polymer concentration:

(a) Aggregation number. In Fig. 7 the variations of N_{agg} with temperature for a 10% solution are plotted. A strong increase from 1 to about 6 for a temperature close to 30 °C can be noted, after which its value rises linearly with temperature. The value of CMT determined here is in good agreement with the result obtained by light-scattering experiment and this result shows that micellization is a slow and continuous process. This could explain why no enthalpic phenomenon was detected by calorimetry.

Representative curves $N_{agg}=C_{te}$ are reported on the phase diagram of the system (Fig. 16). It is important to observe that the aggregation number is a complex function of temperature and initial concentration of polymer. For low values of the aggregation number (for instance $N_{agg}=6$), the curve

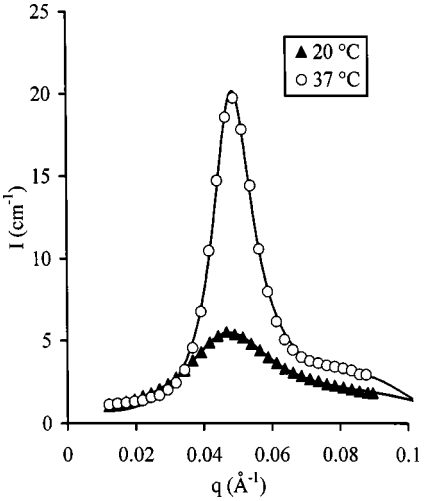

FIG. 15. Scattering function of a 30% solution. The solid lines represent a fit with our model, the symbols are experimental points.

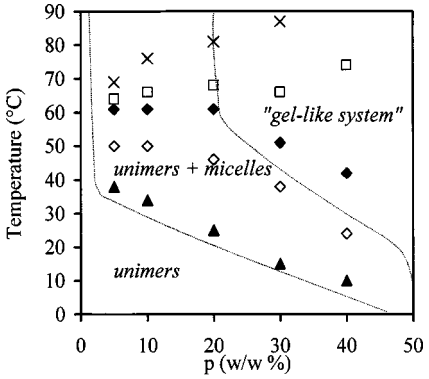

FIG. 16. Examples of curves $N_{agg}=C_{te}$ plotted on the phase diagram. ◇, $N_{agg}=6$; ◇, $N_{agg}=10$; ◆, $N_{agg}=13$; □, $N_{agg}=15$; ×, $N_{agg}=18$.

$N_{agg}=C_{te}$ is parallel to the limit between the ''unimers'' and ''unimers+micelles'' zones, which corresponds to $N_{agg}=1$. Then, the formation of micelles with $N_{agg}<15$ eases as the concentration increases. This result is in agreement with Zhou and Chu's work [25]. The reverse phenomenon is observed when N_{agg} is at a high value (for instance $N_{agg}=18$). This could be due to the high viscosity of the medium, as the migration of unimers to the micelles would require more thermal energy. An intermediate situation was detected for $N_{agg}=15$. The double dependence of the N_{agg} according to temperature and total concentration of polymer in solution has been described by several authors with Pluronic systems [7,8,10,29].

(b) Unimers-micelles equilibrium. Our model also allows the characterization of unimers-micelles equilibrium. We have represented on Fig. 17 the evolution of the concentration of micellized polymer C_m with temperature for different concentrations of T908. The fraction of micellized polymer quickly increases above the CMT and goes to a limiting value C_{max} at high temperatures. C_{max} is equal to about 60% of C whatever the weight percentage p of polymer in solution.

For each concentration and temperature, we have previously assumed in our model that all micelles are identical

$$N_{agg}U \rightleftharpoons 1M$$

where U stands for unimers and M for a micelle containing N_{agg} unimers.

We can define the equilibrium constant K_e by

$$K_e=\frac{[M]_{eq}}{[U]_{eq}^{N_{agg}}},$$

where $[M]_{eq}$ and $[U]_{eq}$ are the molarities at equilibrium expressed in mole per liter,

$$[M]_{eq}=\frac{1000N_m}{N_a}=\frac{1000C_m}{M_wN_{agg}},$$

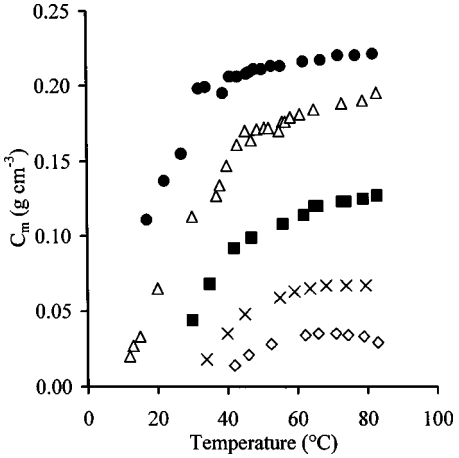

FIG. 17. Evolution of concentration C_m of micellized polymer with temperature for different initial concentrations: ◇, 5%; ×, 10%; ■, 20%; △, 30%; ●, 40%.

$$[U]_{\mathrm{eq}} = 1000\left(\frac{C - C_m}{M_w}\right).$$

In the previous formula, C and C_m are expressed in g cm^{-3}.

We have determined the values of K_e at each temperature and each concentration. If we plot the variations of $\ln(K_e)$ according to the reverse of the absolute temperature for a given concentration, we notice that K_e obeys an Arrhenius law. An example is drawn on Fig. 18 for a 10% solution. We have calculated the activation energy E_a of the process from the slope of the linear fit. In Fig. 19, the value of E_a seems to diverge in the vicinity of $p=2\%$ (i.e., impossible to form micelles) and quickly decreases when the concentration of polymer in solution is increased (formation of micelles eases).

(c) Volume fraction of micelles. In Fig. 20, the different volume fractions of micelles ϕ according to temperature for all solutions studied are plotted. The volume fraction initially abruptly increases with temperature following a linear law. The extrapolation at $\phi=0$ gives the critical temperature of micellization whose value is in good agreement with the results of viscosimetric characterization. It is worth noting that for $p<22\%$, ϕ goes through a maximum value. This result is important because it explains the existence of maximum viscosity for these solutions. For $p\geqslant 30\%$ and at the transition temperature T_c, a discontinuity in the increase of the volume fraction occurs. The values of ϕ at the beginning and end of the discontinuity are respectively equal to 0.41 and 0.49. These values can be compared to those available from theoretical data in the literature. Hoover and Ree have established, using computer simulations, that a hard-sphere fluid with a volume fraction ϕ higher than 0.49 undergoes a transition to a crystalline phase [30]. For ϕ between 0.49 and 0.54, the medium, is a two-phase system (fluid-crystal). For ϕ higher than 0.54, the solution consists of a crystalline phase only. In other words, when a hard-sphere system is gradually compressed, it transforms into a state of long-range order, long before close packing. So, the discontinuity observed could be interpreted as being due to the progressive crystallization of our system even if the experimental values of the limits of transition (0.41 and 0.49) are lower than the theoretical values (0.49 and 0.54). Our results of the micellar volume fractions are in good agreement with those of Mortensen and Pederson for Pluronic P85 solutions [16].

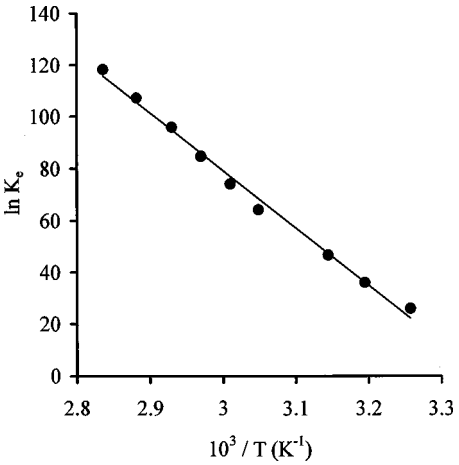

FIG. 18. Arrhenius dependence of equilibrium constant K_e. Representative example of a 10% solution.

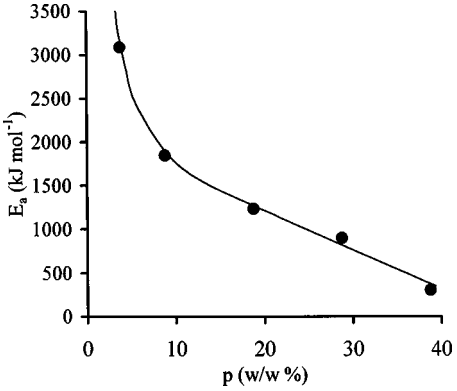

FIG. 19. Variations in activation energy E_a according to initial polymer concentration in solution.

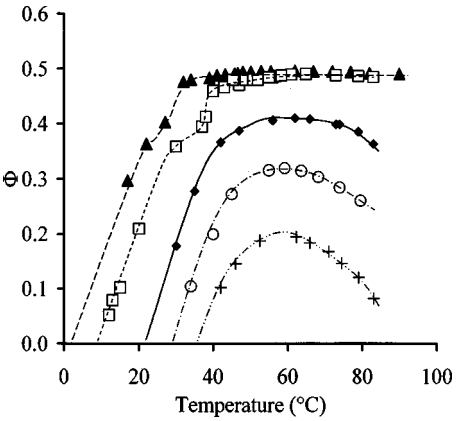

FIG. 20. Evolution of volume fraction of micelles versus temperature for different solutions: +, 5%; ○, 10%; ◆, 20%; □, 30%; ▲, 40%.

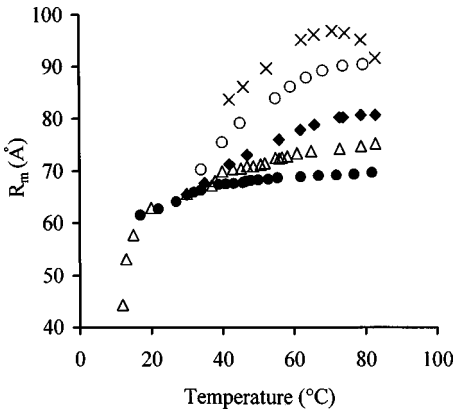

FIG. 21. Temperature effects on the radius of micelles for different solution concentrations. ×, 5%; ○, 10%; ♦, 20%; △, 30%; ●, 40%.

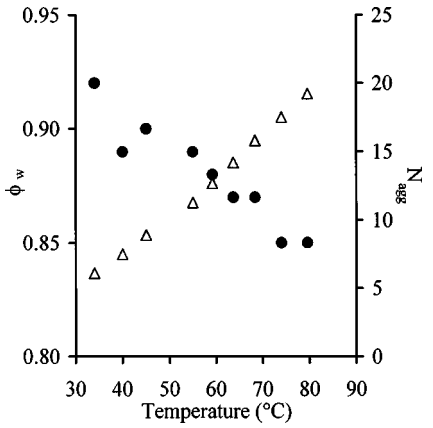

FIG. 22. Evolution of the degree of hydration ϕ_w and N_{agg} versus temperature for a 10% solution. ●, ϕ_w; △, N_{agg}.

For $p=30\%$ or $p=40\%$ and at $T>T_c$ (i.e., in zone 3 of the phase diagram), the micelles are possibly organized in a regular geometric lattice. If we name q_1, q_2, and q_3 the respective values of q at the successive maxima of intensity, the ratios q_2/q_1 and q_3/q_1 are equal to $\sqrt{2}$ and $\sqrt{3}$. This assesses the organization in the medium and would indicate a local cubic structure (Figs. 12 and 13). However, it is relevant to note that the 2D scattering pattern is isotropic. This means that if the micelles organize themselves locally, there is no order at longer distances. In other words, the cubic structures can be oriented in space with any direction.

(d) Size of micelles. The size of the micelles depended strongly on the initial concentration of polymer in solution. This is shown clearly in Fig. 21 where the evolution of radii R_m of the micelles according to temperature and concentration is presented. After a rapid increase above CMT, the size of the micelles tended to a limiting value at a high temperature, which increased when the weight percentage p was decreased. This last result is interesting because it shows that the size of the micelles not only depends on N_{agg}. The degree of hydration ϕ_w of the corona can be deduced from the fraction χ of PEO in the dense layer. In Fig. 22, variations in N_{agg} and ϕ_w with temperature for a 10% solution are plotted. N_{agg} increased linearly while ϕ_w decreased. These opposite evolutions could explain the relative constancy of the radius of micelles R_m observed at high temperatures whatever the concentration.

IV. CONCLUSION

Tetronic 908 in aqueous solutions presented rheological properties, which were strongly dependent on temperature and polymer concentration. This phenomenon is interpreted as a consequence of the amphiphilic character of the polymer. Above critical conditions of temperature or concentration, polymer chains (unimers) aggregated and formed micellar structures as classically observed with other PEO-PPO copolymers such as Pluronic.

The model proposed here shows that micelles can be considered as spherical units with three shells. The central core contains all PPO chains under close-packing conditions, which is surrounded by a dense layer constituted of a fraction χ of PEO chains. The external corona is composed of more or less hydrated PEO units. These micelles soak in a homogenous mixture of unimers and water. This model presents several advantages. First, it satisfactorily describes the experimental curves of the scattered intensity in SANS experiments with a limited number of parameters: the volume fraction ϕ of micelles, their radius R_m, the volume fraction χ of PEO in the dense layer, and the effective concentration C_m of micellized polymer. Second, much structural information can be easily derived and plotted according to temperature or concentration of the polymer. Third, precise correlations between the structure of the material and its rheological properties are possible. For example, at low concentration, the evolution of the volume fraction of micelles explains the viscosity variations of the solution according to temperature.

Comparisons between results from the different experimental techniques employed here were used to understand better the properties of Tetronic 908. For instance, at high temperature and high concentration, secondary peaks from SANS characterizations indicate that micelles are organized and this explains why the solution became gel-like. Spectromechanical measurements complemented this analysis by showing that in reality the mixture behaves like an entangled polymer at these concentrations or temperatures.

Our model can be easily applied to other EO-PO copolymers such as Pluronic or Tetronic systems. Moreover, with few modifications, its methodology may be extended to different materials that form similar micellar structures.

ACKNOWLEDGMENTS

We are grateful to BASF society for providing T908 surfactant. We also thank R. C. Hiorns for his help in the preparation of this manuscript.

[1] G. Wanka, H. Hoffmann, and W. Ulbricht, Colloid Polym. Sci. **268**, 101 (1990).
[2] N. K. Reddy, P. J. Fordham, D. Attwood, and C. Booth, J. Chem. Soc., Faraday Trans. **86**, 1569 (1990).
[3] P. Bahadur and K. Pandya, Langmuir **8**, 2666 (1992).
[4] S. Hvidt, Colloids Surf., B **112**, 201 (1995).
[5] V. Lenaerts, C. Triqueneaux, M. Quarton, F. Rieg-Falson, and P. Couvreur, Int. J. Pharm. **39**, 121 (1987).
[6] O. Glatter, G. Scherf, K. Schillen, and W. Brown, Macromolecules **27**, 6046 (1994).
[7] W. Brown, K. Schillén, M. Almgren, S. Hvidt, and P. Bahadur, J. Phys. Chem. **95**, 1850 (1991).
[8] S. L. Nolan, R. J. Phillips, P. M. Cotts, and S. R. Dungan, J. Colloid Interface Sci. **191**, 291 (1997).
[9] G. E. Yu, Y. W. Yang, Z. Yang, D. Attwood, C. Booth, and V. M. Nace, Langmuir **12**, 4697 (1996).
[10] S. Zhou, J. Su, and B. Chu, J. Polym. Sci. **36**, 889 (1998).
[11] B. Jeong, D. S. Lee, J. Shon, Y. H. Bae, and S. W. Kim, J. Polym. Sci. **37**, 751 (1999).
[12] S. M. King, R. K. Heenan, V. M. Cloke, and C. Washington, Macromolecules **30**, 6215 (1997).
[13] L. Meilleur, A. Hardy, and F. Quirion, Langmuir **12**, 4697 (1996).
[14] K. Schillén, W. Brown, and C. Konak, Macromolecules **26**, 3611 (1993).
[15] K. Mortensen, W. Brown, and E. Jorgensen, Macromolecules **27**, 5654 (1994).
[16] K. Mortensen and J. S. Pedersen, Macromolecules **26**, 805 (1993).
[17] K. Mortensen, J. Phys. Condens. Matter **8**, A103 (1996).
[18] Y. C. Liu, S. H. Chen, and J. S. Huang, Phys. Rev. E **54**, 1698 (1996).
[19] L. Goldminst, F. K. von Gottberg, K. A. Smith, and T. A. Hatton, Langmuir **13**, 3659 (1997).
[20] L. Goldminst, G. Y. Yu, C. Booth, K. A. Smith, and T. A. Hatton, Langmuir **15**, 1651 (1999).
[21] P. Hickl, M. Ballauff, P. Lindner, and A. Jada, Colloid Polym. Sci. **275**, 1027 (1997).
[22] C. Wu, T. Liu, and B. Chu, Macromolecules **30**, 4574 (1997).
[23] B. Chu, G. Wu, and D. K. Schneider, J. Polym. Sci., Part B: Polym. Phys. **32**, 2605 (1994).
[24] R. K. Prud'homme, G. Wu, and D. K. Schneider, Langmuir **12**, 4651 (1996).
[25] Z. Zhou and B. Chu, Macromolecules **27**, 2025 (1994).
[26] J. R. Lopes and W. Loh, Langmuir **14**, 750 (1998).
[27] P. Alexandridis, J. F. Holzwarth, and T. A. Hatton, Macromolecules **27**, 2414 (1994).
[28] E. Caponetti, M. A. Floriano, M. Varisco, and R. Triolo, in *Structure and Dynamics of Strongly Interacting Colloids and Supramolecular Aggregates in Solution*, edited by S. H. Chen, J. S. Huang, and P. Tartaglia (Kluwer Academic, London, 1992), Vol. C 369, p. 535.
[29] P. Linse, Macromolecules **27**, 6404 (1994).
[30] W. Hoover and F. H. Ree, J. Chem. Phys. **49**, 3609 (1968).